Journal of Materials Chemistry C

Materials for optical and electronic devices

www.rsc.org/MaterialsC

Volume 1 | Number 42 | 14 November 2013 | Pages 6915–7118

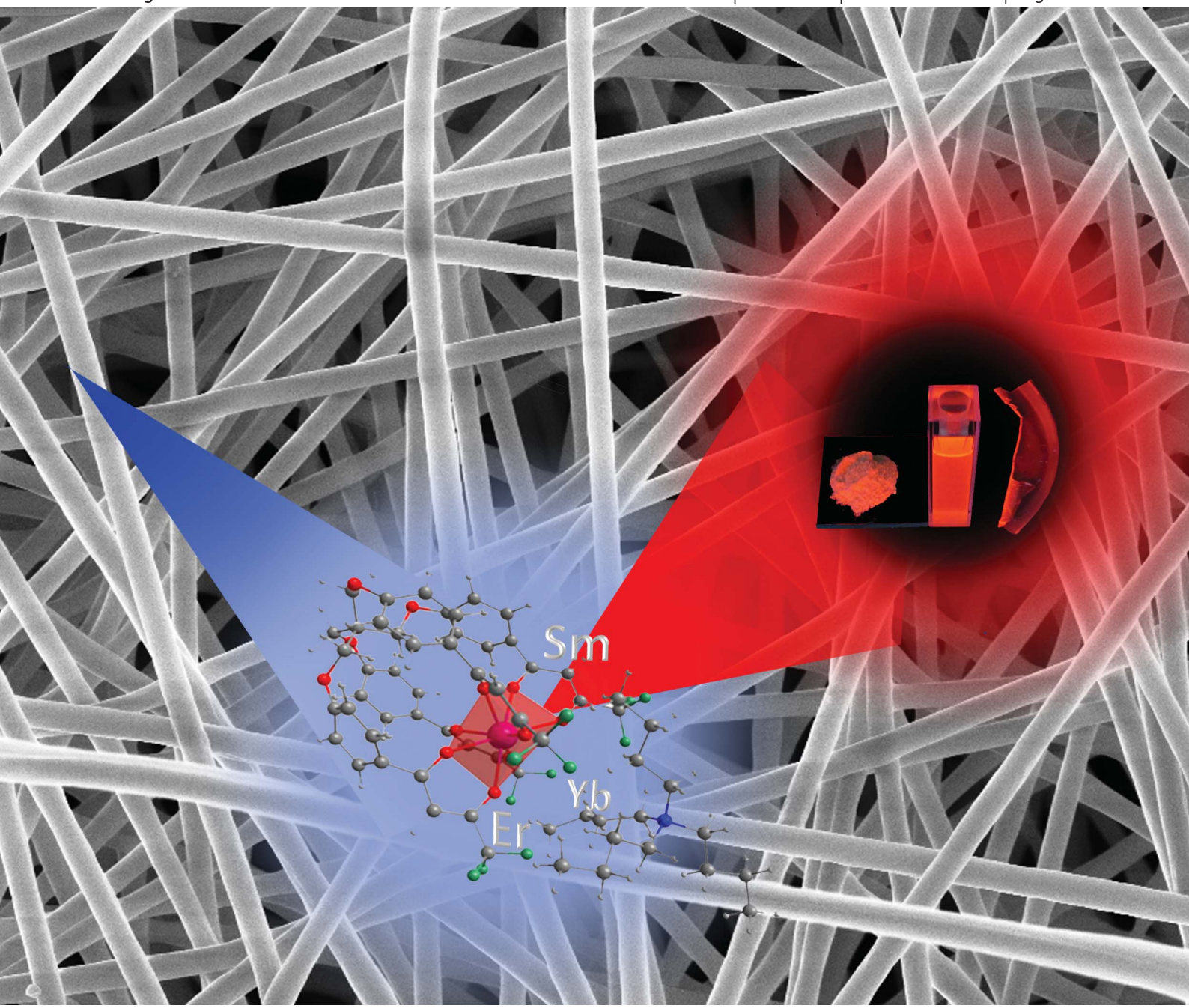

ISSN 2050-7526

RSC Publishing

PAPER

Silvanose Biju, Jean-Claude G. Bünzli, Hwan Kyu Kim *et al.*

A new tetrakis β-diketone ligand for NIR emitting Ln^{III} ions: luminescent doped PMMA films and flexible resins for advanced photonic applications

Journal of Materials Chemistry C

RSC Publishing

PAPER

A new tetrakis β-diketone ligand for NIR emitting Ln^{III} ions: luminescent doped PMMA films and flexible resins for advanced photonic applications†

Cite this: *J. Mater. Chem. C*, 2013, **1**, 6935

Silvanose Biju,*[a] Yu Kyung Eom,[a] Jean-Claude G. Bünzli*[ab] and Hwan Kyu Kim*[a]

A new antenna molecule containing four benzoyltrifluoroacetone (BTFA) moieties anchored to a single carbon atom and connected through four flexible methoxy groups, namely 1,1′-(4,4′-(2,2-bis((4-(4,4,4-trifluoro-3-oxobutanoyl)phenoxy)methyl) propane-1,3-diyl)bis(oxy)bis(4,1-phenylene))bis(4,4,4-trifluorobutane-1,3-dione) [$\mathbf{H_4L}$], has been designed and synthesized. Using this ligand, a series of homo- and hetero-metallic Ln^{III} complexes of general formula [LnL]NBu_4 (where Ln = Sm (**1**), Gd (**2**), Er (**3**), Yb (**4**), $Er_{0.5}Yb_{0.5}$ (**5**), $Er_{0.5}Gd_{0.5}$ (**6**), $Yb_{0.5}Gd_{0.5}$ (**7**) and NBu_4 = tetrabutyl ammonium) have been isolated. All these complexes have high molar absorption coefficients (>40 000 M^{-1} cm^{-1} around 330 nm in DMF) and display strong visible (Sm^{III}) and/or, NIR (Sm^{III}, Er^{III}, Yb^{III}) luminescence in solid state and in DMF solution upon irradiation at the ligand-centred bands in the range 250–400 nm. Furthermore, these complexes have been doped into PMMA matrices yielding highly luminescent, photo-stable films and flexible resins made of fibres with average diameter 300–400 nm. Photoluminescence studies show that the newly designed ligand is an adequate sensitizer for Sm^{III}, Yb^{III} and Er^{III} luminescence. The emission quantum yields and the luminescence lifetimes at room-temperature are 3.4 ± 0.5% and 79.1 ± 1 μs for Sm^{III} and 2.6 ± 0.4% and 12.1 ± 0.1 μs for Yb^{III} in solid state. Furthermore the overall quantum yields and lifetime measurements for the mixed metallic complex show that Yb^{III} → Er^{III} energy transfer occurs resulting in enhanced Er^{III} emission.

Received 19th June 2013
Accepted 17th August 2013

DOI: 10.1039/c3tc31181c

www.rsc.org/MaterialsC

Introduction

Initially, interest for near-infrared (NIR) emitting Ln^{III} ions stemmed from the development of optical fibres, lasers and amplifiers[1] since the NIR emission of Er^{III} around 1.5 μm is in the so-called telecommunication "C" window. The subsequent implementation of upconverted nanophosphors for the detection of cell and tissue antigens[2] added a whole new field of applications for Ln^{III} NIR luminescence. As a result, ions such as Er^{III} and Yb^{III} (emitting at 980 nm and a good sensitizer of Er^{III} emission) are attracting considerable research attention due to their characteristic luminescence properties.[1,3] These properties, coupled with the advantage of good signal transmittance of NIR radiation by silica and biological tissues, make them attractive for potential use in a number of photonic applications including telecommunications, medical diagnosis and imaging, as well as in security inks and counterfeiting tags.[2] Trivalent samarium is another lanthanide ion which has several transitions in the range 800–1700 nm (ref. 4–6) along with intense orange red luminescence in the visible region.[4,7,8] Usually, the small absorption cross-sections of Ln^{III} ions result in inefficient emission from their 4f levels under direct excitation unless powerful lasers are used. One of the most popular ways to overcome this limitation is by complexing the Ln^{III} ions with organic ligands that sensitize the emission of the metal ion by the well-known antenna effect.[9–11] However NIR emitting lanthanide complexes with organic ligands often show low emission efficiencies and shorter excited state lifetime values compared to inorganic systems due to multiphonon de-excitation caused by the coupling of the f levels with high-frequency oscillators like O–H, N–H and C–H, present in the organic ligands or in the solvent molecules.[3,12] Careful selection of solvents and clever design of ligands can easily minimize the number of O–H and N–H groups around the Ln^{III} ions but C–H bonds are very difficult to eliminate from an organic molecule. Fluorinated β-diketones are one among the most studied antenna molecules for NIR emitting Ln^{III} ions, in view of the minimum number of C–H vibrators present; however the electron attractive nature of the C–F bonds often reduces the

[a]*Department of Advanced Materials Chemistry and WCU Center for Next Generation Photovoltaic Systems, Korea University, Jochiwon-eup, Sejong-si, 339-700, Republic of Korea. E-mail: hkk777@korea.ac.kr; drbijusilvanose@gmail.com; Fax: +82-44-860-1331; Tel: +82-44-860-1493*

[b]*Institute of Chemical Sciences and Engineering, École Polytechnique Fédérale de Lausanne, BCH 1402, CH-1015 Lausanne, Switzerland. E-mail: jean-claude.bunzli@epfl.ch; Fax: +41 21 693 5550; Tel: +41 21 693 9821*

† Electronic supplementary information (ESI) available: NMR, EDS and PL data. See DOI: 10.1039/c3tc31181c

coordination ability of these molecules.[13,14] Moreover, in most of the reports, bidentate β-diketonates result in the formation of neutral tris Ln^{III} complexes with the metal coordination sphere completed by either solvent molecules with O–H vibrators or neutral donors with large numbers of C–H oscillators.[13,14]

To solve this problem, we have designed a new fluorinated β-diketone podand ($\mathbf{H_4L}$) by combining four well known fluorinated benzoyltrifluoroacetone (BTFA) moieties anchored to a single carbon atom and connected by four methoxy groups to ensure enough flexibility for the four diketonates to be able to simultaneously coordinate the metal ion. Indeed, this molecule is expected to form octa-coordinated anionic Ln^{III}-β-diketonates similar to the tetrakis(β-diketonates) with bidentate ligands, which are known to be more luminescent than the tris complexes.[15] The grafting of four coordination units onto a single framework is expected to lead to larger chelate effect and therefore higher binding constants compared to the parent.

For practical applications in optical devices it is often advantageous to incorporate the luminescent Ln^{III} centres into inert hosts like silica matrices, which in addition to combining the properties of both organic and inorganic compounds ensure better long-term stability and easier processability.[16] Covalent grafting of ligands onto the backbone of silica networks like MCM-41,[5,17] SBA-15[17,18] and xerogels[19] *via* Si–C bonds is one of the most common methods for generating homogeneous hybrid materials with high mechanical stability. McCoy *et al.* developed pH sensitive hydrogels based on the Eu^{III}-quinoline cyclen conjugate complex.[20] Recently our group has developed a new class of organic–inorganic hybrids based on a hierarchically ordered mesoporous organosilica, which shows sensitized emission from Er^{III} and Yb^{III} centres.[21] However the NIR luminescence efficiencies of Ln^{III} complexes in silica matrices remain unimpressive in view of the O–H oscillators present in the second coordination sphere.[22] Another class of hybrid materials, namely lanthanide–polymer hybrids, which combines the good luminescent properties of lanthanide complexes with the excellent mechanical processing properties of organic polymers, seems to be better suited and is therefore attracting hefty attention.[1] These materials find applications as plastic optical fibres, lasing materials, and optical amplifiers.[1] A widely used polymer host for luminescent lanthanide complexes is poly-(methyl methacrylate) (PMMA) which is a low-cost, simply prepared polymer with excellent optical properties.[23,24] Thus, in the present work, we have doped the newly developed visible and NIR emitting complexes into this matrix to get highly transparent films that can also be electrospun into resins consisting of uniform wires of diameter 300–400 nm. The optical properties of the newly synthesized complexes and hybrid materials are reported and discussed.

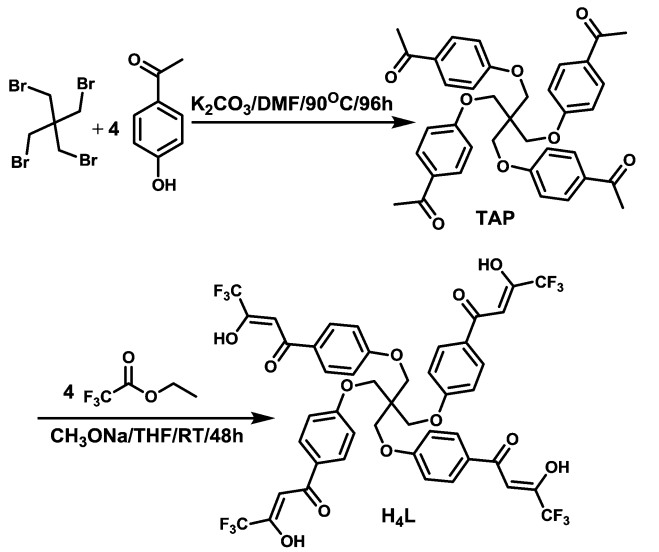

Scheme 1 Synthetic procedure for the ligand $\mathbf{H_4L}$.

Results and discussion

Spectroscopic characterization of H_4L and $[LnL]NBu_4$ (1–7)

The synthetic procedures adopted for the ligand $\mathbf{H_4L}$ and its Ln^{III} complexes (**1–7**) are described in Schemes 1 and 2, respectively. The ^1H and ^{13}C NMR spectra of $\mathbf{H_4L}$ are presented in Fig. S1 and S2 (ESI†). Vibrational spectroscopy and microanalysis data for **1–7** demonstrate that the Ln^{3+} : L^{4-} mole ratio is 1 : 1 and that one molecule of counter ion (Bu_4N^+) is present. The carbonyl stretching frequency ν_s(C=O) of $\mathbf{H_4L}$ (1600 cm^{-1}) shifts to 1623–1626 cm^{-1} in **1–7** along with the appearance of a new peak in the range 1678–1681 cm^{-1}, thus indicating coordination of the carbonyl groups to the Ln^{III} cation in each case. Furthermore, the presence of signals in the range 2800–2900 cm^{-1} due to the $-CH_2-$ groups and the signal around 1015–1017 cm^{-1}, ν_s(C–N), confirm the presence of NBu_4^+ in all isolated complexes. The absence of any broad bands around 3500 cm^{-1} ν_s(O–H) in **1–7** proves that they are anhydrous and, therefore, that all four β-diketonate moieties are coordinated to the Ln^{III} cations. The thermal stability of the complexes was examined by means of thermogravimetric analysis and typical thermograms are depicted in Fig. 1. All the complexes display two distinct decomposition steps. The first one, around 100 °C, occurs with weight losses of 1.5–2% and is related to the removal of adsorbed solvent molecules. Further thermal decomposition of **1–7** appears to be more complex, with steps around 210, 400, 600 and 700 °C corresponding to the loss of organic groups and formation of the metal oxides. The residual weight is between 15 and 16% that is approximately equal to the weight of rare-earth oxides (calcd: 12.7–14.0%). Most importantly, the thermal stability of these complexes is as high as 210 °C and none of them shows distinct weight losses in the range 150–175 °C, as expected for complexes without solvent molecules in the first coordination sphere.

Ligand-centred luminescence and energy levels

The complexes described in this study were soluble only in highly polar solvents such as DMF and DMSO. The highly coordinating DMSO can destroy the Ln^{III} coordination sphere in Ln^{III}-β-diketonates. Hence solution studies were conducted in the less coordinating DMF medium. The UV-vis absorption spectra of ligand $\mathbf{H_4L}$ and its Ln^{III} complexes **1–4** in DMF

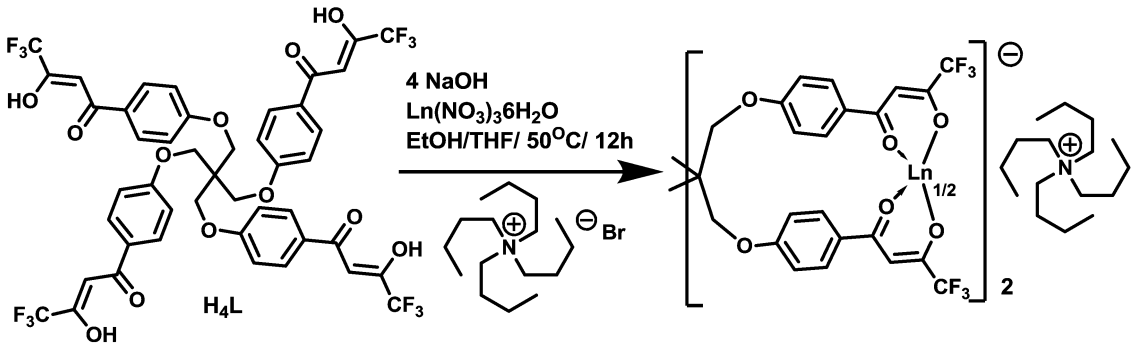

Scheme 2 Synthetic procedure for lanthanide complexes [LnL]NBu_4 [Ln = Sm (**1**), Gd (**2**), Er (**3**), Yb (**4**), $Er_{0.5}Yb_{0.5}$ (**5**), $Er_{0.5}Gd_{0.5}$ (**6**), $Yb_{0.5}Gd_{0.5}$ (**7**)].

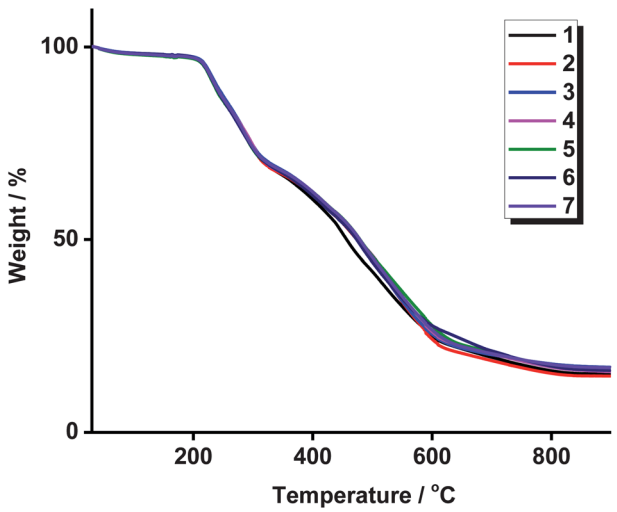

Fig. 1 Thermogravimetric curves of Ln^{III} complexes **1–7**.

solutions (Fig. 2a) and in PMMA (Fig. 2b) were recorded at room temperature. Relevant data are gathered in Table 1. The absorption spectrum of $\mathbf{H_4L}$ shows two maxima at 323 nm and 272 nm with large molar absorption coefficients (~40–42 000 M^{-1} cm^{-1}) and a shoulder at 285 nm. The peak around 323 nm can be attributed to the singlet–singlet ($^1\pi$–π^*) enolic transitions of the β-diketone moieties[25] while the features at lower wavelengths are due to singlet–singlet ($^1\pi$–π^*) transitions in the phenyl rings.[26] The absorption spectra of the Ln^{III} complexes are similar to that of $\mathbf{H_4L}$ except for a blue shift of the shoulder at 285 nm to 278 nm and a red shift of the 323 nm absorption to 329 nm. This is in accordance with the fact that the conjugation in the β-diketonate moieties becomes larger upon coordination with Ln^{III} ions. Furthermore the molar absorption coefficients of the lowest-energy transition calculated for **1–4** (~42–44 000 M^{-1} cm^{-1}) are similar and close to the value for the free ligand, pointing to the presence of one L^{4-} anion bonded to each Ln^{III} cation. The energy of the singlet state level of the ligand was calculated from the higher absorption wavelength edge of the absorption spectrum of **2**, and is equal to 26 700 cm^{-1} (375 nm). The absorption spectra of thin films of PMMA doped with 4 wt% of **1**, **3** and **4** are broader than those in DMF solution with two well resolved signals around 328 and 274 nm. The overall shapes of the absorption spectra in DMF and PMMA are, however, similar and hence one can assume that the absorbing species remain the same in both media. A first conclusion is that these complexes can efficiently absorb UV radiations and may be interesting as UV-protection coatings and/or wavelength-converting materials.

It is known that the energy absorbed by the ligand-centred absorption bands in Ln^{III} complexes can undergo intersystem crossing leading to enhanced population of its lowest triplet level and subsequent energy transfer to the nearby Ln^{III}-centred 4f states.[27] This mechanism works for most of the Ln^{III}

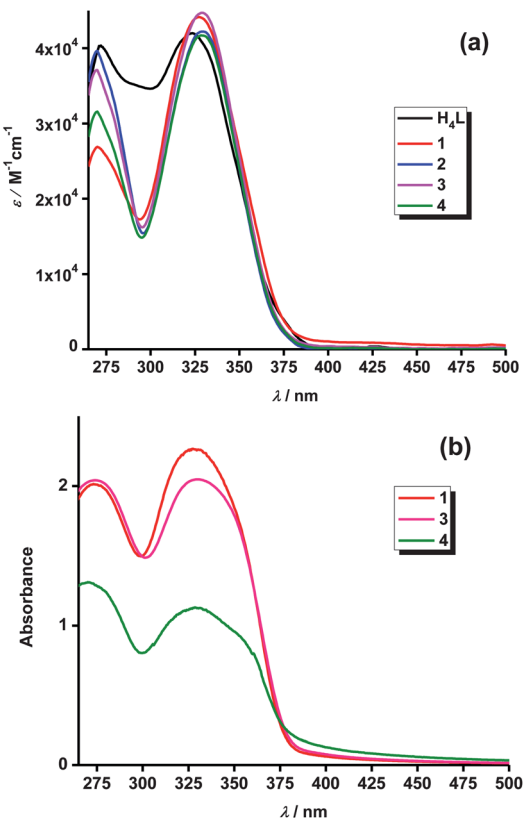

Fig. 2 UV-vis absorption spectra (298 K) of (a) the ligand and its Ln^{III}-complexes in DMF ($c \approx 10^{-6}$ M) and (b) Ln^{III} complexes doped into PMMA films (4 wt%); the thickness of the films is not the same for all samples and varies from 0.6 to 0.9 mm.

Table 1 UV-vis absorption spectral data (298 K) of the ligand and its Ln^{III}-complexes in DMF ($c \approx 2 \times 10^{-6}$ M) and in PMMA films

Compound	λ_{max}/nm (ε/M^{-1} cm^{-1})
H_4L	323 (42 000), 272 (40 360)
1	329 (44 240), 270 (26 899)
2	329 (42 442), 270 (39 250)
3	329 (42 442), 270 (37 093)
4	329 (41 931), 270 (31 562)
1/PMMA 4 wt%	328, 274
3/PMMA 4 wt%	328, 273
4/PMMA 4 wt%	328, 273

complexes except the one containing Gd^{III} because its lowest excited level, $^8S_{7/2}$, is located at 32 150 cm^{-1}, well above the triplet states of most organic chromophores. Thus investigation of the luminescence spectra of the Gd^{III} complex **2** gives useful information about the ligand states.[28,29] Fig. 3 displays the fluorescence spectra of H_4L and **2** at 298 K as well as the phosphorescence spectrum of **2** at 77 K obtained by excitation at their absorption maxima. As is evident from this figure, the emission maximum of H_4L (428 nm) is substantially red shifted in the luminescence and phosphorescence spectra of **2** (500 nm). However, the luminescence spectrum of **2** at 298 K shows a shoulder around 430 nm corresponding to fluorescence emission that disappears completely in the phosphorescence spectrum recorded at 77 K with a time delay of 0.05 ms. Thus the emission band centred at 500 nm can be considered as the emission from the triplet ($^3\pi$–π^*) state of bound L^{4-}. The low-temperature phosphorescence spectrum of **2** could be decomposed into four Gaussian components at 469 nm (21 321 cm^{-1}), 500 nm (20 000 cm^{-1}), 552 nm (18 115 cm^{-1}) and 633 nm (15 797 cm^{-1}). The most energetic component is assigned to the 0-phonon transition. With this at hand, ligand-to-metal energy transfer pathways can be predicted as follows; they are sketched in Fig. 4. The energy difference between the $^3\pi$–π^* state of L^{4-} and the receiving $Sm^{III}(^4G_{5/2})$ level is ~3400 cm^{-1} and hence one may expect a reasonably efficient sensitization of the luminescence of this ion. In a similar way the $Er(^2H_{11/2})$ level located at 19 100 cm^{-1} or other Er^{III} levels such as $^4S_{3/2}$ or $^4F_{9/2}$ can accept energy from the triplet state of L^{4-}; subsequent intra-ion non-radiative processes can then lead to population of the emitting $^4I_{13/2}$ level. The situation for Yb^{III} is not simple and may involve a mechanism assisted through the divalent state by electron transfer, which necessitates an energy of about 19 000 cm^{-1}.[3]

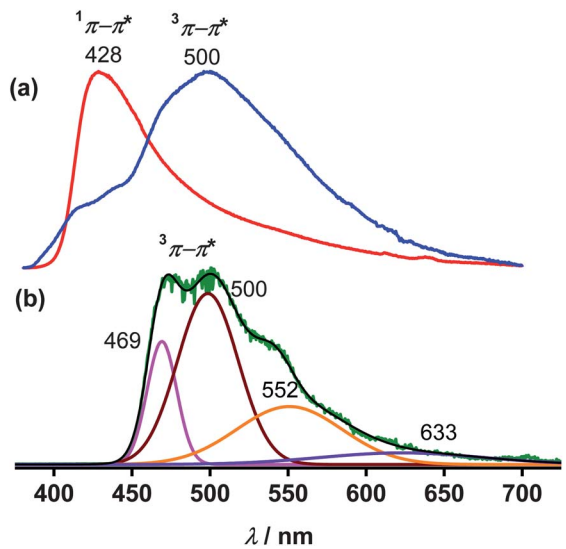

Fig. 3 (a) Corrected fluorescence spectra of H_4L (red curve) and **2** (blue curve) at 298 K, in solid state, and (b) corrected phosphorescence spectrum of **2** at 77 K and its decomposition into Gaussian components (dispersion in $CDCl_3$, $c \approx 10^{-5}$ M, delay increment 0.05 ms, $\lambda_{ex} = 330$ nm); vertical scales are arbitrary units.

Ln^{III}-centred photophysical properties of homometallic complexes

In order to determine the best excitation wavelength for each Ln^{III} complex, excitation spectra were recorded by monitoring the emission wavelengths at 645 nm (Sm^{III}), 1545 nm (Er^{III}) and 983 nm (Yb^{III}). The spectra recorded for solid-state samples are

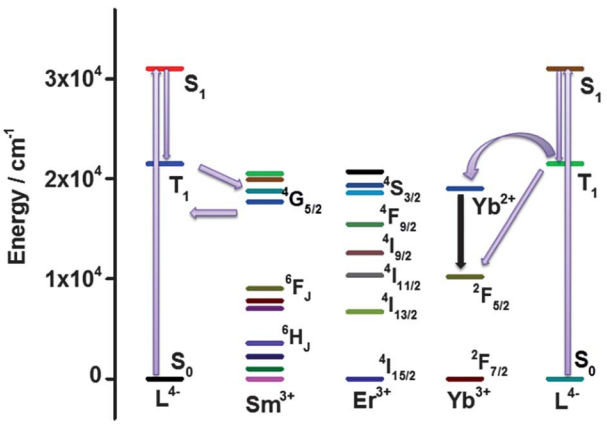

Fig. 4 Energy diagram for L^{4-} and relevant Ln^{III} ions.

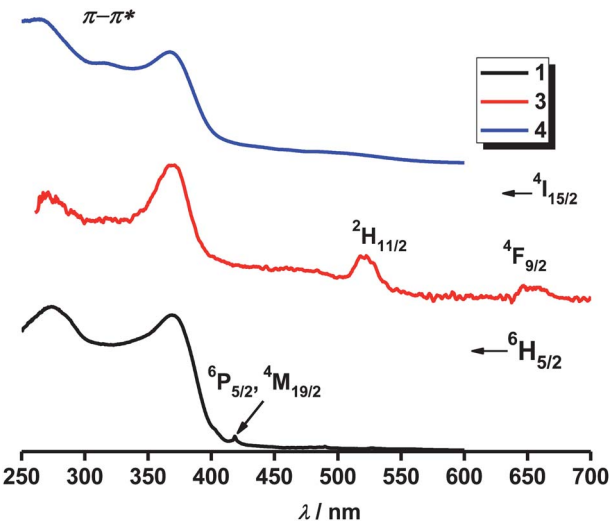

Fig. 5 Excitation spectra of Ln^{III} complexes **1**, **3**, and **4** in solid state at 298 K; emission monitored at 645 nm (**1**), 1545 nm (**3**) and 983 nm (**4**); vertical scale: arbitrary units.

shown in Fig. 5, while those measured in DMF solutions and in PMMA matrices are displayed in Fig. S3 and S4, respectively (ESI†). All these spectra are dominated by typical ligand-centred broad bands covering the entire UV region with a tail extending into the blue, up to 400 nm. The excitation spectra of solid-state samples of **1**, **3**, and **4** present two maxima, one around 360–370 nm and the other around 270–280 nm, as well as a shoulder around 320 nm. In addition to these broad bands some faint f–f transitions are also observed: $^6P_{5/2}$, $^4M_{19/2} \leftarrow {}^6H_{5/2}$ at 418 nm (Sm^{III}),[8] $^2H_{11/2} \leftarrow {}^4I_{15/2}$ at 522 nm and $^4F_{9/2} \leftarrow {}^4I_{15/2}$ at 654 nm (Er^{III}).[30] The very low intensities of these bands compared to the ligand-centred bands suggest that an antenna mechanism is operative in all complexes. The solid-state excitation spectrum of the Yb^{III} complex **4** shows an additional broad and faint band centred at 500 nm that could reflect a contribution from the electron-transfer mechanism involving Yb^{II}. The excitation spectra recorded in DMF solution are similar for all Ln^{III} ions but are substantially different in shape compared to the solid-state spectra: the most prominent feature is at 314–318 nm, corresponding to the shoulder in the solid-state spectra, while the two other maxima lie at 275–280 and 350–355 nm. The spectra of **1**, **3** and **4** in PMMA matrices resemble those in DMF solution with, however, broader bands. No lanthanide-centred excitation bands are seen in these two media, pointing to a more efficient antenna mechanism compared to solid state.

When excited through the ligand-centred band at 315 nm, the Sm^{III} complex emits typical narrow f–f bands in both visible and NIR spectral ranges (Fig. 6). The spectra obtained are identical in shape and peak positions whatever the medium is. The observed bands are assigned to transitions from the $^4G_{5/2}$ excited state to the lower energy levels of ^6H_J (J = 5/2, 7/2, 9/2, and 11/2) in the visible[8] and ^6F_J (J = 5/2, 7/2, and 9/2)[5] in the NIR. In comparison with the magnetic dipole transition $^4G_{5/2} \rightarrow {}^6H_{7/2}$ at 602 nm, the electric dipole transition $^4G_{5/2} \rightarrow {}^6H_{9/2}$ at 645 nm is much more intense and is responsible for the orange-red emission colour.[7] The intensity ratio between these two transitions, $I(^4G_{5/2} \rightarrow {}^6H_{9/2})/I(^4G_{5/2} \rightarrow {}^6H_{7/2})$, is identical in all media, within experimental errors: 3.86 in solid state, 3.83 in DMF and 3.84 in PMMA. This indicates that the local environment around the Sm^{III} ion remains the same in all samples.

The emission spectra of the Er^{III} and Yb^{III} complexes **3** and **4** cover both the visible (ligand emission centred at 500 nm, Fig. S5, ESI†) and the NIR spectral ranges (Fig. 7). While the visible emission spectrum of **4** resembles the one of the Gd^{III} complex, the spectrum of **3** features a structured dip at 520 nm which can be assigned to absorption from the Er^{III} ion through the $^2H_{11/2} \leftarrow {}^4I_{15/2}$ hypersensitive transition. This, together with the intensity of the ligand emission band being much smaller in both **3** and **4** than in **2**, clearly indicates that energy transfer from L^{4-} to Er^{III} and Yb^{III} is operative. This conclusion is further confirmed by the lifetime of the triplet state of L^{4-} which, at 77 K, is reduced to <50 μs in complexes **3** and **4** from 845 ± 5 μs in the Gd^{III} compound, pointing to the role of the triplet state as the feeding level.

The NIR emission spectra of complexes **3** and **4** in the three media studied are very similar at 298 K (Fig. 7) with bands in the range 1460–1640 nm (maximum at 1545 nm, shoulders at 1500 and 1600 nm) for **3** and 930–1090 nm (maximum at 983 nm, shoulders at 1003 and 1026 nm) for **4**. They are due to the $Er(^4I_{13/2} \rightarrow {}^4I_{15/2})$ and $Yb(^2F_{5/2} \rightarrow {}^2F_{7/2})$ transitions with splitting attributable to crystal field effects.[5,17,31,32] Furthermore, a weak anti-Stoke band around 950 nm is also present in the room temperature emission spectrum of **4** but is absent from the 77 K spectrum, which confirms its "hot band" nature.[33] The spectra recorded at low temperature (Fig. 8) have better resolution and crystal field components are easily spotted at 1545, 1585, and 1615 nm for Er^{III} and 983, 1005, and 1030 nm for Yb^{III}.[30] The observation of only 3 crystal field components for $Yb(^2F_{7/2})$ is compatible with a cubic arrangement of the coordinating atoms around the metal ion. Finally, the solid-state sample of the Yb^{III} complex shows visible-light sensitized NIR emission when excited at 500 nm, both at 298 K and 77 K.

The efficiency of visible and NIR emission of complexes **1**, **3**, and **4** can be examined in terms of overall quantum yields (Φ_{ov})

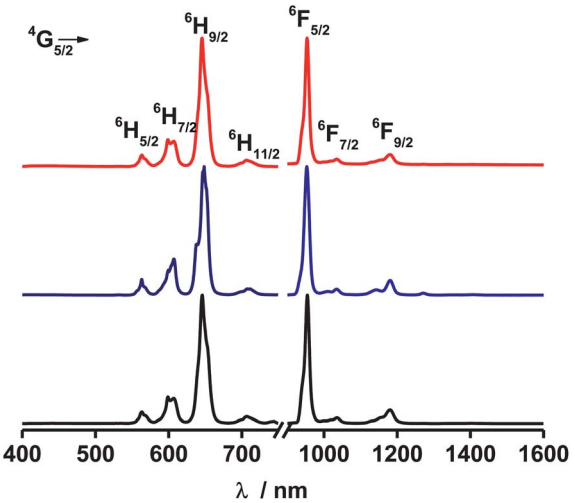

Fig. 6 Corrected emission spectra of **1** at 298 K in solid state (black curve, λ_{ex} = 365 nm), in DMF (blue curve; $c = 10^{-5}$ M, λ_{ex} = 315 nm) and in a 4 wt%-doped PMMA film (red curve, λ_{ex} = 365 nm); vertical scales: arbitrary units.

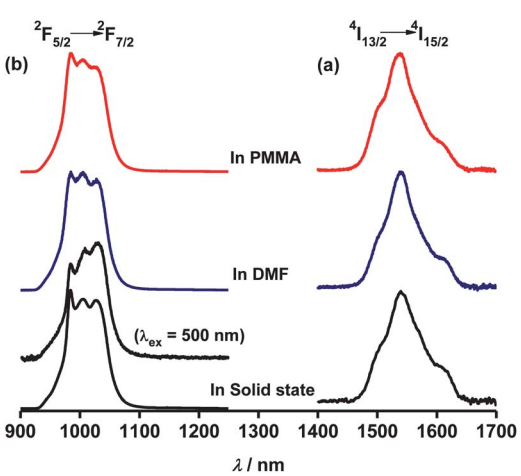

Fig. 7 Corrected NIR emission spectra of (a) **3**, and (b) **4** at 298 K in solid state (black curves, λ_{ex} = 365 nm), in DMF (blue curves; $c = 10^{-5}$ M, λ_{ex} = 315 nm) and in 4 wt% doped PMMA films (red curves, λ_{ex} = 365 nm): vertical scales: arbitrary units.

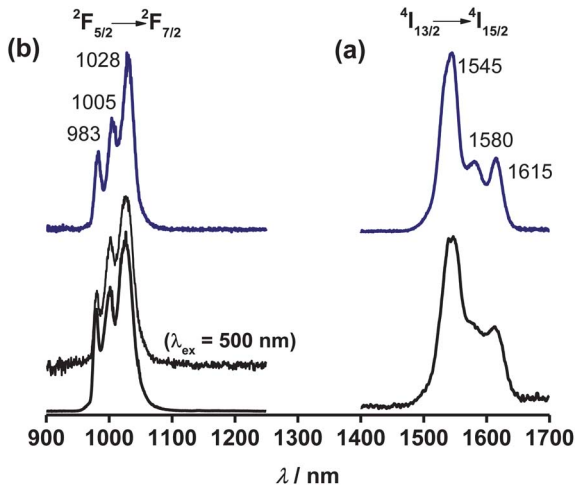

Fig. 8 Corrected NIR emission spectra of (a) **3**, and (b) **4** at 77 K in solid state (black curves, $\lambda_{ex} = 365$ nm), and in DMF (blue curves; $c = 10^{-5}$ M, $\lambda_{ex} = 315$ nm): vertical scales: arbitrary units.

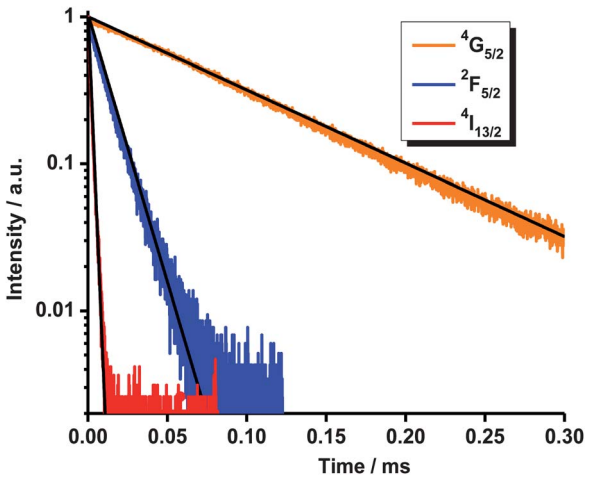

Fig. 9 Decay profiles of complexes **1** (orange curve), **3** (red curve), and **4** (blue curve), in solid state at 298 K.

and excited state lifetimes (τ_{obs}). The overall quantum yield is regulated by the sensitization efficiency of the antenna molecule (ϕ_{sen}) and the intrinsic luminescence quantum yield of the Ln^{III} ion (ϕ_{Ln}): $\Phi_{ov} = \phi_{sen}\phi_{Ln}$.[4] Data for Φ_{ov} for samples **1** and **4** have been determined at room temperature and are listed in Table 2. In the case of Sm^{III}, transitions in the visible region only have been taken into consideration. The excited-state lifetime of complexes **1**, **3**, and **4** at 298 K (τ_{obs}) has been investigated by exciting the samples using a 355 nm pulsed laser line and monitoring the NIR transitions $^4G_{5/2} \rightarrow {}^6F_{5/2}$ at ~953 nm (Sm^{III}), $^4I_{13/2} \rightarrow {}^4I_{15/2}$ at ~1545 nm (Er^{III}) and $^2F_{5/2} \rightarrow {}^2F_{7/2}$ at ~983 nm (Yb^{III}), respectively. All the decay curves could be fitted with single exponential functions, consistent with the presence of a single major luminescent species in the complexes. Calculated values are given in Table 2 and typical decay profiles obtained for the solid-state samples are shown in Fig. 9. As expected, the Sm^{III} complex has the highest values in all media for Φ_{ov} and τ_{obs} compared to Er^{III} and Yb^{III} while Φ_{ov} could not be measured for Er^{III} due to the too low emission intensity. Introduction of the complexes into PMMA leads to mixed effects: it is beneficial for Sm^{III} which then features the largest quantum yield measured, but the excited state lifetime is shortened by about 8 and 20% compared to solid state for Sm^{III} and Yb^{III} while it remains constant for Er^{III}. On the other hand, there are no drastic differences in lifetimes between solid-state samples and DMF solutions for the three Ln^{III} ions, suggesting that the local environment around the metal ions remains the same, hence proving that the complexes are stable in DMF solution. The Φ_{ov} and τ_{obs} data listed here for the Yb^{III} complex **4** are, to the best of our knowledge, the highest values reported for anhydrous Yb^{III} complexes with fluorinated β-diketonates[34] (Table 3). However, these values are not as high as the values published for complexes with benzoyl-substituted 8-hydroxyquinolines.[35] Compared to [Yb(BTFA)phen], complex **4** shows 2.8 times larger Φ_{ov} and 1.2 times longer τ_{obs} in solution, which can be attributed to the suppression of the formation of potential conformers arising from rotations of the phenyl groups around a single bond, which are restricted in L^{4-} compared to BTFA.

Table 2 Excited-state lifetimes (τ_{obs}) and overall quantum yields (Φ_{ov}) of complexes **1**, **3**, and **4** at 298 K

	1		**3**	**4**	
Complex	Φ_{ov} (%)	τ_{obs} (μs)	τ_{obs} (μs)	Φ_{ov} (%)	τ_{obs} (μs)
Solid	3.4 ± 0.5	79.1 ± 0.1	1.6 ± 0.1	2.6 ± 0.4	12.1 ± 0.1
DMF	2.5 ± 0.4	72.5 ± 0.1	1.5 ± 0.1	1.8 ± 0.3	12.3 ± 0.1
PMMA film	4.0 ± 0.6	72.7 ± 0.1	1.6 ± 0.1	n.d.	9.7 ± 0.1
PMMA wires	4.0 ± 0.6	73.1 ± 0.1	1.6 ± 0.1	n.d.	9.8 ± 0.1

One of the main disadvantages of PMMA films or sheets is their brittleness, due to the high glass transition temperature. To remedy this problem, Binnemans and co-workers produced flexible polymer films with high luminescence efficiencies by blending the polymer with a plasticizer.[23] It is also known that when the diameter of polymeric fibre materials is shrunk to sub-micrometers or nanometers, there appear several amazing characteristics such as a very large surface area to volume ratio, flexibility in surface functionalities, and superior mechanical performance like stiffness and tensile strength compared with any other known form of the material. These outstanding properties make the polymer nanofibres optimal candidates for several important applications.[36] Thus PMMA solutions doped with 4 wt% of complexes **1**, **3**, and **4** were electrospun to fabricate flexible resins. Electron microscopy images reveal the presence of uniform wires of diameter 300–400 nm (Fig. 10). The photoluminescent properties of these wires are similar to those of doped films as demonstrated by the excitation and emission spectra displayed in Fig. S6 (ESI†) and 11, respectively, as well as by overall quantum yield and excited-state lifetime data (Table 2).

Ln^{III}-centred photophysical properties of heterometallic compounds

The Yb^{III} ion has one order of magnitude higher absorption cross-section at 980 nm than Er^{III}. Hence co-doping materials with both Er^{III} and Yb^{III} ions is a usual method to improve the

Table 3 Photophysical data for Yb^{III}-β-diketonate complexes at room temperature reported in the literature[a]

	Φ_{ov} (%)		τ_{obs} (μs)			
Complex	Solid State	Toluene	Solid state	Toluene	PMMA	Ref.
$[YbL]NBu_4$ (**4**)	2.6 ± 0.4	1.8 ± 0.3[b]	12.1 ± 0.1	12.3 ± 0.1[b]	9.7 ± 0.1	This work
$[Yb(TTA)_3(phen)]$	1.6 ± 0.2	1.1 ± 0.1	12.01 ± 0.02	10.4	10.7	13 and 34
$[Yb(THFP)_3(phen)]$	—	1.20	—	11.7	11.1	34
$[Yb(TTDFH)_3(phen)]$	—	0.88	—	11.8	11.0	34
$[Yb(BTFA)_3(phen)]$	—	0.65	—	10.4	—	34
$[Yb(BHFP)_3(phen)]$	—	0.88	—	10.7	—	34
$[Yb(BTDFA)_3(phen)]$	—	0.98	—	11.0	—	34
$[Yb(BHDFD)_3(phen)]$	—	0.92	—	10.5	—	34

[a] TTA = 2-thenoyltrifluoroacetone, THFP = 2-thenoylheptafluoropentanone, TTDFO = 2-thenoyltridecylfluorooctanone, BTFA = benzoyltrifluoroacetone, BHFP = benzoylheptafluoropentanone, BTDFO = benzoyltridecylfluorooctanone, BHDFD = benzoylheptadecylfluorodecanone, phen = 1,10-phenanthroline. [b] Measured in DMF ($c = 10^{-5}$ M).

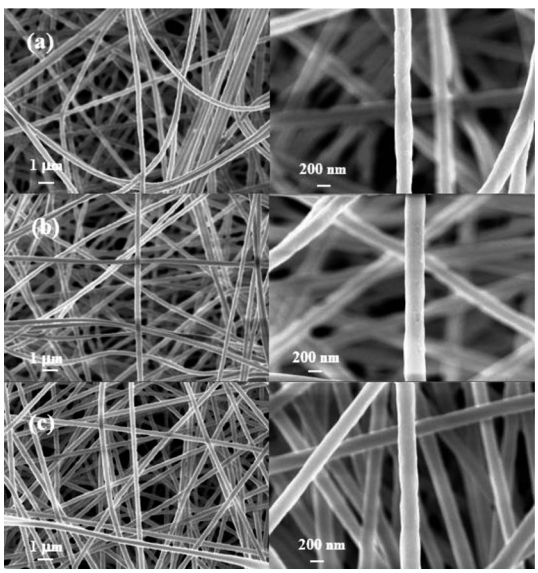

Fig. 10 SEM images of **1** (a), **3** (b) and **4** (c) doped PMMA resins (4 wt%). Magnification: × 15 000, scale bar = 1 μm (left); × 50 000, scale bar = 200 nm (right).

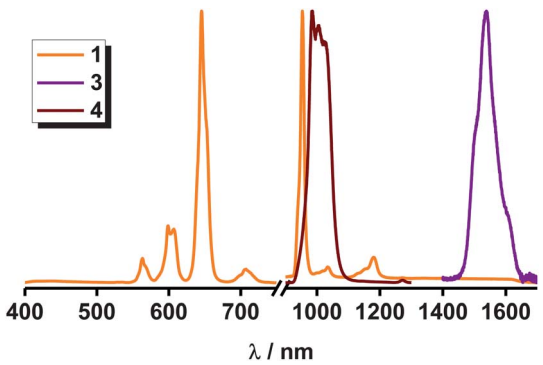

Fig. 11 Corrected emission spectra of **1**, **3**, and **4** doped into PMMA fibres (4 wt %) at 298 K. Vertical scale: arbitrary units.

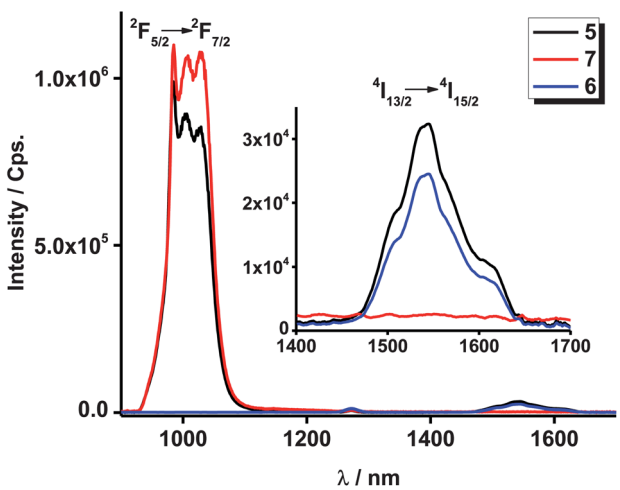

Fig. 12 Corrected emission spectra of **5–7** at 298 K in solid state, inset: Er^{III} emission.

pumping efficiency of Er^{III} ions.[14] Indirect excitation of the Er^{III} ions occurs mainly *via* energy transfer from the $Yb(^2F_{5/2})$ level to the $Er(^4I_{11/2}, {}^4I_{13/2})$ levels. Thus we have synthesized the heterobimetallic complex $[Er_{0.5}Yb_{0.5}L]NBu_4$ (**5**) and, for comparison purposes, $[Er_{0.5}Gd_{0.5}L]NBu_4$ (**6**) and $[Gd_{0.5}Yb_{0.5}L]NBu_4$ (**7**). The atomic ratios between different lanthanides present in each of the complexes were confirmed by EDS analysis (Fig. S7 and Table S1, ESI†). The excitation spectra of **5** obtained by monitoring the emission signals around 1545 nm (Er^{III}) and 983 nm (Yb^{III}) are similar to those of its pure counterparts **3** and **4**, and are dominated by the ligand centred band with main maximum at 365 nm (Fig. S8, ESI†). When excited at this wavelength, the emission spectrum of **5** shows transitions related to both Er^{III} and Yb^{III} centres (Fig. 12). The strength of the Er^{III} transition is much weaker than that of the Yb^{III} signal; however it has larger luminescence intensity (+60%) than complex **6**. On the other hand, a decrease in the intensity of the Yb^{III}-centred emission (−20%) is observed in comparison with that of complex **7**. This fact is related to energy transfer between the Yb^{III} and Er^{III} ions, since the $^4I_{13/2}$ level of Er^{III} (6500 cm^{-1}) lies ~3500 cm^{-1} below the $Yb(^2F_{5/2})$ level. This conclusion is substantiated by the values of overall quantum yields and excited state lifetimes: for

Yb^{III}, $\Phi_{ov} = 1.4 \pm 0.2\%$ and $\tau_{obs} = 9.4 \pm 0.1$ μs are smaller than the values obtained for **7** ($\Phi_{ov} = 1.6 \pm 0.2\%$ and $\tau_{obs} = 10.3 \pm 0.1$ μs). On the other hand the excited-state lifetimes obtained for the Er^{III} luminescence in complexes **5** (1.5 ± 0.1 μs) and **6** (1.6 ± 0.1 μs) are identical, within experimental errors. The Yb^{III}-to-Er^{III} energy transfer efficiency in the mixed metallic complex **5** can be computed from $\phi_{Ln \rightarrow Ln} = 1 - (\chi/\chi_0)$[37,38] where χ and χ_0 are the quantum yields or lifetimes of the $Yb^{III}(^2F_{5/2})$ level in the presence and absence of acceptor, respectively. The $\phi_{Ln \rightarrow Ln}$ values obtained by taking these two parameters into account are in reasonable agreement: 12.5 and 8.9%, respectively.

Conclusions

We have designed a novel podand featuring four fluorinated β-diketone arms derived from benzoyltrifluoroacetone which forms 1 : 1 complexes with trivalent lanthanide ions, saturating their coordination sphere. Photoluminescence studies show that the newly designed antenna molecule is highly efficient in sensitizing Sm^{III} (both in the visible and NIR ranges) and Yb^{III} luminescence and can provide sizable sensitization for Er^{III} ions. The emission quantum yields and the luminescence lifetimes at room-temperature obtained for the Yb^{III} complex in the present study are the highest among many Yb^{III} complexes with fluorinated β-diketonate ligands. Furthermore $Yb^{III} \rightarrow Er^{III}$ energy transfer is used as a tool to improve the emission intensity of the Er^{III} transition around 1.5 μm in a hetero-bimetallic complex. The complexes can be easily doped into PMMA matrices to give luminescent, photo-stable films and flexible resins under the form of wires. In addition to these interesting emission properties, the novel hybrid materials reported here have large absorption coefficient in the entire UV range and in the blue, up to 400 nm, that make them potential candidates as UV-protection coatings, wavelength converting materials in photovoltaics, or for optical amplification in the field of telecommunications.

Experimental section

Materials

Lanthanide(III) nitrate hexahydrates, 99.9%, were obtained from Sigma Aldrich (Ln = Sm, Gd, Er, Yb). 4-Hydroxyacetophenone 99.9% (Sigma Aldrich), 1,3-dibromo-2,2-bis(bromomethyl)propane 99.9% (Sigma Aldrich), ethyltrifluoroacetate 99.9% (Sigma Aldrich), tetra-*n*-butylammoniumbromide $(C_4H_9)_4NBr$ 99.9% (Acros Organics), polymethyl methacrylate (PMMA) (Alfa Aesar), and sodium methoxide 99.9% (Sigma Aldrich) were used without further purification. Solvents were dried using standard methods. All the other chemicals used were of analytical reagent grade.

Synthesis of the ligand H_4L

The ligand **H_4L** was prepared by a two-step process with an overall yield of 95% (Scheme 1). In the first step, a mixture of 1,3-dibromo-2,2-bis(bromomethyl)propane (1.25 mmol), 4-hydroxyacetophenone (5 mmol), and K_2CO_3 (5.10 mmol) in dry dimethylformamide (DMF, 20 mL) was stirred and heated at 90 °C for 96 h. The hot mixture was cooled, diluted with H_2O (20 mL) and the product was extracted with $CHCl_3$ (2 × 35 mL). The $CHCl_3$ layer was washed with H_2O and brine and was then dried over anhydrous Na_2SO_4. The product was obtained as a pale yellow solid by precipitation from hexane (250 mL). In the second step the tetraacetylphenone synthesized in the first step (1.25 mmol) and NaOMe (5 mmol) were added to 20 mL of dry tetrahydrofuran (THF) and stirred for 10 min at room temperature. To this solution, ethyltrifluoroacetate (5 mmol) was added dropwise in an inert atmosphere and stirred for 48 h. To the resulting solution, 50 mL of 2 M HCl were added, and the mixture was extracted twice with dichloromethane (2 × 35 mL). The organic layer was separated and dried over Na_2SO_4, and the product was obtained by precipitation upon addition of hexane (250 mL).

H_4L (pale yellow solid). Yield: 95%. Anal. calcd for $C_{45}H_{32}F_{12}O_{12}$ (992.71): C, 54.45; H, 3.25; found: C, 54.79; H, 3.39. FTIR (KBr, cm^{-1}): 3450 (ν_s O–H); 3071 (ν $C_{sp2}H$); 2956, 2886 (ν $C_{sp3}H$); 1600 (ν_s C=O); 1509, 1464, 1312 (ν C=C); 1267, 1065 (ν_s C–O); 1172, 1145 (δ C–H); 1110 (ν_s C–F); 845, 794 (δ C–H); 704 (δ CF_3). ^1H NMR ($CDCl_3$, 300 MHz), δ (ppm): 4.48 (8H, s), 6.48 (4H, s), 7.03 (8H, d; $J = 9.0$), 2.92 (8H, d; $J = 8.7$), 15.31 (4H, s: broad). ^{13}C NMR ($CDCl_3$, 300 MHz) δ (ppm): 44.99 (C); 66.52(–O–CH_2–); 91.78 (CO–CH–CO); 115.50, 126.38, 130.13, 163.05 (phenyl); 126.39 (CF_3); 176.36, 188.72 (CO). $m/z = 1081.11$ [M − 4H+ 4Na + H]$^+$.

Synthesis of the Ln^{III} complexes [LnL]NBu_4

To an ethanolic suspension of **H_4L** (10 mL), 4 mmol of aqueous NaOH (2 M) were added at room temperature and the mixture was stirred until complete dissolution of **H_4L**. Required volumes of aqueous Ln^{III} nitrates were then added slowly and the solution was diluted to 50 mL with THF. The reaction mixture was then stirred for 6 h at 50 °C. A solution of Bu_4NBr (1.05 mmol) in deionized water/THF (5/10 mL) was then added, resulting in the formation of a precipitate (Scheme 2). After stirring the mixture for 6 h at 50 °C, the pale yellow solid product was filtered, washed with *n*-hexane, and dried. The obtained [LnL]NBu_4 complexes were re-dissolved in DMF, filtered and the filtrate was allowed to stand for a period of 3–4 weeks. The [LnL]NBu_4 complexes were obtained as yellow powders and were dried in a vacuum at 50 °C for 2 days. Yield: 90–95%. The limited solubility of $LnLNBu_4$ in common organic solvents prevented the isolation of single crystals suitable for X-ray analysis: the complexes are soluble only in DMF and DMSO and efforts to grow single crystals from solvent combinations involving DMF and DMSO were not successful.

[SmL]NBu_4 (1) (yellow solid). Yield: 92%. Anal. calcd for $C_{61}H_{64}F_{12}NO_{12}Sm$ (1381.50): C, 53.03; H, 4.67; N, 1.01; found: C, 53.21; H, 4.79; N, 1.10. FTIR (KBr, cm^{-1}): 3072 (ν $C_{sp2}H$); 2964, 2940, 2878 (ν $C_{sp3}H$); 1681, 1623 (ν_s C=O); 1597, 1505, 1468, 1309 (ν C=C); 1288, 1240 (ν_s C–O); 1173, 1125 (δ C–H); 1118 (ν_s C–F); 1019 (ν_s C–N); 842, 783 (δ C–H); 703 (δ CF_3).

[GdL]NBu_4 (2) (yellow solid). Yield: 95%. Anal. calcd for $C_{61}H_{64}F_{12}GdNO_{12}$ (1388.39): C, 52.77; H, 4.65; N, 1.01; found: C,

52.91; H, 4.80; N, 1.07. FTIR (KBr, cm^{-1}): 3071 (ν $C_{sp2}H$); 2965, 2938, 2876 (ν $C_{sp3}H$); 1678, 1625 (ν_s C=O); 1598, 1500, 1471, 1308 (ν C=C); 1288, 1244 (ν_s C–O); 1173, 1124 (δ C–H); 1118 (ν_s C–F); 1015 (ν_s C–N); 840, 781 (δ C–H); 704 (δ CF_3).

[ErL]NBu_4 (3) (yellow solid). Yield: 95%. Anal. calcd for $C_{61}H_{64}ErF_{12}NO_{12}$ (1398.40): C, 52.39; H, 4.61; N, 1.00; found: C, 52.51; H, 4.81; N, 1.05. FTIR (KBr, cm^{-1}): 3070 (ν $C_{sp2}H$); 2965, 2940, 2877 (ν $C_{sp3}H$); 1678, 1626 (ν_s C=O); 1598, 1500, 1470, 1308 (ν C=C); 1288, 1245 (ν_s C–O); 1173, 1124 (δ C–H); 1118 (ν_s C–F); 1017 (ν_s C–N); 840, 781 (δ C–H); 704 (δ CF_3).

[YbL]NBu_4 (4) (yellow solid). Yield: 95%. Anal. calcd for $C_{61}H_{64}F_{12}NO_{12}Yb$ (1404.18): C, 52.18; H, 4.59; N, 1.00; found: C, 52.41; H, 4.77; N, 1.10. FTIR (KBr, cm^{-1}): 3069 (ν $C_{sp2}H$); 2965, 2939, 2877 (ν $C_{sp3}H$); 1678, 1625 (ν_s C=O); 1598, 1501, 1470, 1308 (ν C=C); 1288, 1244 (ν_s C–O); 1173, 1124 (δ C–H); 1118 (ν_s C–F); 1016 (ν_s C–N); 840, 781 (δ C–H); 702 (δ CF_3).

[$Er_{0.5}Yb_{0.5}$L]NBu_4 (5) (yellow solid). Yield: 95%. Anal. calcd for $C_{61}H_{64}Er_{0.5}F_{12}NO_{12}Yb_{0.5}$ (1401.29): C, 52.28; H, 4.60; N, 1.00; found: C, 52.40; H, 4.70; N, 1.10. FTIR (KBr, cm^{-1}): 3071 (ν $C_{sp2}H$); 2965, 2937, 2877 (ν $C_{sp3}H$); 1678, 1625 (ν_s C=O); 1599, 1500, 1470, 1308 (ν C=C); 1288, 1246 (ν_s C–O); 1173, 1124 (δ C–H); 1118 (ν_s C–F); 1015 (ν_s C–N); 841, 781 (δ C–H); 704 (δ CF_3).

[$Er_{0.5}Gd_{0.5}$L]NBu_4 (6) (yellow solid). Yield: 95%. Anal. calcd for $C_{61}H_{64}$ $Er_{0.5}F_{12}$ $Gd_{0.5}NO_{12}$ (1393. 40): C, 52.58; H, 4.63; N, 1.01; found: C, 52.80; H, 4.75; N, 1.06. FTIR (KBr, cm^{-1}): 3071 (ν $C_{sp2}H$); 2965, 2938, 2878 (ν $C_{sp3}H$); 1678, 1626 (ν_s C=O); 1598, 1500, 1472, 1308 (ν C=C); 1288, 1244 (ν_s C–O); 1173, 1124 (δ C–H); 1119 (ν_s C–F); 1015 (ν_s C–N); 840, 781 (δ C–H); 703 (δ CF_3).

[$Yb_{0.5}Gd_{0.5}$]LNBu_4 (7) (yellow solid). Yield: 95%. Anal. Calcd for $C_{61}H_{64}F_{12}Gd_{0.5}NO_{12}Yb_{0.5}$ (1396. 29): C, 52.47; H, 4.62; N, 1.00; found: C, 52.72; H, 4.81; N, 1.10. FTIR (KBr, cm^{-1}): 3070 (ν $C_{sp2}H$); 2966, 2938, 2877 (ν $C_{sp3}H$); 1679, 1626 (ν_s C=O); 1598, 1500, 1470, 1308 (ν C=C); 1288, 1245 (ν_s C–O); 1174, 1124 (δ C–H); 1118 (ν_s C–F); 1016 (ν_s C–N); 840, 781 (δ C–H); 705 (δ CF_3).

Methods

Elemental analyses were performed with a Perkin-Elmer Series 2 Elemental Analyzer 2400. A Perkin-Elmer Spectrum One FT-IR spectrometer using KBr (neat) was used to obtain the IR spectral data. Mass spectrum of the ligand **H_4L** was recorded on a JEOL JSM 600 fast atom bombardment high resolution mass spectrometer (FABMS) and the thermogravimetric analyses were performed on a TGA-50H instrument (Shimadzu, Japan). SEM and EDS analyses were performed on a JEOL JSM-5600LV microscope. Absorption spectra of the ligands and complexes were recorded in DMF solution and PMMA films on a UV-2450 spectrophotometer (Shimadzu). Photoluminescence spectra were collected on a Fluorolog FL 3-22 spectrometer from Horiba-Jobin Yvon-Spex equipped for both visible and NIR measurements and were corrected for the instrumental function. NIR luminescence studies were conducted under Ar atmosphere. Powdered samples were put into 2 mm i.d. quartz capillaries. The PMMA films with size $\sim 10 \times 5$ mm were used as such. Overall quantum yield data for Sm^{III} in the visible spectral range and for Yb^{III} in NIR were acquired at rt on the same instrument using a home-modified integrating sphere;[39] for Yb^{III}, a solid state sample of [Yb$(TTA)_3$(phen)] was used as standard (Φ_{ov}=1.6%).[13] The values reported are averages of 6 different measurements with an estimated error of ±15%. NIR luminescence lifetimes were measured with a previously described instrumental setup.[40] The PMMA films were obtained by drop casting and the resins were prepared with the eS-Robot electrospinning system from NanoNc Co. Ltd, Korea. DMF solutions of PMMA doped with 4 wt% of Ln^{III} complexes were taken in a syringe with a needle of gauge 23 G and electrospun by applying a voltage of 8 kV between the solution and the counter electrode kept at a distance of 10 cm.

Acknowledgements

This research was supported by the World Class University Program funded by the Ministry of Education, Science, and Technology through the National Research Foundation of Korea (grant R31-2012-000-10035-0), and by a grant from Korea University (2010). One of the authors (S. B.) thanks Collegiate Education Dept. and Dept. of Higher Education Govt. of Kerala, India for granting leave without allowance for doing post-doctoral research.

Notes and references

1 K. Kuriki, Y. Koike and Y. Okamoto, *Chem. Rev.*, 2002, **102**, 2347–2356.
2 H. J. M. A. A. Zijlmans, J. Bonnet, J. Burton, K. Kardos, T. Vail, R. S. Niedbala and H. J. Tanke, *Anal. Biochem.*, 1999, **267**, 30–36.
3 S. Comby and J.-C. G. Bünzli, in *Handbook on the Physics and Chemistry of Rare Earths*, ed. K. A. Gschneidner Jr, J.-C. G. Bünzli and V. K. Pecharsky, Elsevier, 2007, pp. 217–470.
4 S. Quici, M. Cavazzini, G. Marzanni, G. Accorsi, N. Armaroli, B. Ventura and F. Barigelletti, *Inorg. Chem.*, 2005, **44**, 529–537.
5 L.-N. Sun, J.-B. Yu, H.-J. Zhang, Q.-G. Meng, E. Ma, C.-Y. Peng and K.-Y. Yang, *Microporous Mesoporous Mater.*, 2007, **98**, 156–165.
6 B. Chu, W. L. Li, Z. R. Hong, F. X. Zang, H. Z. Wei, D. Y. Wang, M. T. Li, C. S. Lee and S. T. Lee, *J. Phys. D: Appl. Phys.*, 2006, **39**, 4549–4552.
7 K. Miyata, T. Nakagawa, R. Kawakami, Y. Kita, K. Sugimoto, T. Nakashima, T. Harada, T. Kawai and Y. Hasegawa, *Chem.–Eur. J.*, 2011, **17**, 521–528.
8 X. Y. Chen, M. P. Jensen and G. K. Liu, *J. Phys. Chem. B*, 2005, **109**, 13991–13999.
9 S. I. Weissman, *J. Chem. Phys.*, 1942, **10**, 214–217.
10 N. Sabbatini, M. Guardigli and J.-M. Lehn, *Coord. Chem. Rev.*, 1993, **123**, 201–228.
11 J.-M. Lehn, *Angew. Chem., Int. Ed.*, 1990, **29**, 1304–1319.
12 I. Hernandez, Y.-X. Zheng, M. Motevalli, R. H. C. Tan, W. P. Gillin and P. B. Wyatt, *Chem. Commun.*, 2013, **49**, 1933–1935.
13 L. N. Puntus, K. J. Schenk and J.-C. G. Bünzli, *Eur. J. Inorg. Chem.*, 2005, 4739–4744.
14 Q. Zhong, H. Wang, G. Qian, Z. Wang, J. Zhang, J. Qiu and M. Wang, *Inorg. Chem.*, 2006, **45**, 4537–4543.

15 K. Binnemans, *Chem. Rev.*, 2009, **109**, 4283–4374.
16 B. Yan, *RSC Adv.*, 2012, **2**, 9304–9324.
17 L.-N. Sun, H.-J. Zhang, C.-Y. Peng, J.-B. Yu, Q.-G. Meng, L.-S. Fu, F.-Y. Liu and X.-M. Guo, *J. Phys. Chem. B*, 2006, **110**, 7249–7258.
18 L.-N. Sun, H.-J. Zhang, J.-B. Yu, S.-Y. Yu, C.-Y. Peng, S. Dang, X.-M. Guo and J. Feng, *Langmuir*, 2008, **24**, 5500–5507.
19 B. Tong, S. Wang, Y. Meng and B. Wang, *Photochem. Photobiol. Sci.*, 2007, **6**, 519–520.
20 C. P. McCoy, F. Stomeo, S. E. Plush and T. Gunnlaugsson, *Chem. Mater.*, 2006, **18**, 4336–4343.
21 S. Biju, Y. K. Eom, J.-C. G. Bunzli and H. K. Kim, *J. Mater. Chem. C*, 2013, **1**, 3454–3466.
22 A. Mech, A. Monguzzi, F. Meinardi, J. Mezyk, G. Macchi and R. Tubino, *J. Am. Chem. Soc.*, 2010, **132**, 4574–4576.
23 K. Lunstroot, K. Driesen, P. Nockemann, L. Viau, P. H. Mutin, A. Vioux and K. Binnemans, *Phys. Chem. Chem. Phys.*, 2010, **12**, 1879–1885.
24 Y. Hasegawa, M. Yamamuro, Y. Wada, N. Kanehisa, Y. Kai and S. Yanagida, *J. Phys. Chem. A*, 2003, **107**, 1697–1702.
25 S. Biju, D. B. A. Raj, M. L. P. Reddy and B. M. Kariuki, *Inorg. Chem.*, 2006, **45**, 10651–10660.
26 H.-F. Li, P.-F. Yan, P. Chen, Y. Wang, H. Xu and G.-M. Li, *Dalton Trans.*, 2012, **41**, 900–907.
27 G. A. Crosby, R. E. Whan and R. M. Alire, *J. Chem. Phys.*, 1961, **34**, 743–748.
28 S. Biju, M. L. P. Reddy, A. H. Cowley and K. V. Vasudevan, *J. Mater. Chem.*, 2009, **19**, 5179–5187.
29 N. S. Baek, M. K. Nah, Y. H. Kim and H. K. Kim, *J. Lumin.*, 2007, **127**, 707–712.
30 C. Reinhard and H. U. Güdel, *Inorg. Chem.*, 2002, **41**, 1048–1055.
31 L.-N. Sun, J.-B. Yu, G.-L. Zheng, H.-J. Zhang, Q.-G. Meng, C.-Y. Peng, L.-S. Fu, F.-Y. Liu and Y.-N. Yu, *Eur. J. Inorg. Chem.*, 2006, 3962–3973.
32 J. Zhang and S. Petoud, *Chem.–Eur. J.*, 2008, **14**, 1264–1272.
33 F. R. Gonçalves e Silva, O. L. Malta, C. Reinhard, H.-U. Güdel, C. Piguet, J. E. Moser and J.-C. G. Bünzli, *J. Phys. Chem. A*, 2002, **106**, 1670–1677.
34 M. P. Tsvirko, S. B. Meshkova, V. Y. Venchikov, Z. M. Topilova and D. V. Bol'shoi, *Opt. Spectrosc.*, 2001, **90**, 669–673.
35 N. M. Shavaleev, R. Scopelliti, F. Gumy and J.-C. G. Bünzli, *Inorg. Chem.*, 2009, **48**, 7937–7946.
36 Z.-M. Huanga, Y.-Z. Zhangb, M. Kotakic and S. Ramakrishna, *Comp. Sci. Technol.*, 2003, **63**, 2223–2253.
37 S. Biju, D. B. Ambili Raj, M. L. P. Reddy, C. K. Jayasankar, A. H. Cowley and M. Findlater, *J. Mater. Chem.*, 2009, **19**, 1425–1432.
38 D. Ananias, M. Kostova, F. A. Almeida Paz, A. Ferreira, L. D. Carlos, J. Klinowski and J. Rocha, *J. Am. Chem. Soc.*, 2004, **126**, 10410–10417.
39 A. Aebischer, F. Gumy and J.-C. G. Bünzli, *Phys. Chem. Chem. Phys.*, 2009, **11**, 1346–1353.
40 N. M. Shavaleev, R. Scopelliti, F. Gumy and J.-C. G. Bünzli, *Inorg. Chem.*, 2008, **47**, 9055–9068.